Reprinted from May 1989, Vol. 111, Journal of Heat Transfer

Thermal Measurements in Large Pool Fires

J. J. Gregory

N. R. Keltner

R. Mata, Jr.

Thermal Test and Analysis Division,
Sandia National Laboratories,
Albuquerque, NM 87185

During the summer of 1983, a series of pool fire tests was conducted in which the test item was a 1.4-m-dia, 6.4-m-long, mild steel calorimeter with a mass of approximately 10,000 kg. The purpose of these tests was to study the thermal response of a large test item in a specified fire configuration, to define thermal boundary conditions, and to assess the repeatability of the fire environment. While the calorimeter used in the tests simulated a nuclear waste transportation cask, the results of the study have broader application to the truck and rail transport of hydrocarbon fuels and hazardous chemicals.

Introduction

There is an interest in determining the response and survivability of a variety of items when subjected to large fires, which might occur in a transportation accident or petrochemical industry accident. Specifications for conducting simulated transportation accident tests are given by the International Atomic Energy Agency (IAEA, 1985) and the U.S. Nuclear Regulatory Commission (NRC, 1983).

The thermal environment in a large open pool fire is not well defined. The highly turbulent nature of a large open pool fire and its susceptibility to winds produces temperature and flow fields that are very nonuniform in both space and time. Complete and representative theoretical models that describe the environment are not available.

The tests described in this paper involved a large cylindrical test item in a hydrocarbon pool fire configured along the guidelines of the IAEA and NRC specifications. To address the question of the repeatability of the pool fire environment and provide empirical information that could aid in modeling it, three tests were performed using identical instrumentation. A large calorimeter was used to represent a physically large, thermally massive shipping cask. Complete details of this test program are given by Gregory et al. (1987).

Test Description

The series of three half-hour tests was conducted in a 9.1 m by 18.3 m by 0.9 m deep concrete pool. The test item was a large calorimeter supported by a steel stand such that the bottom was 0.9 m above the initial level of the fuel in accordance with NRC guidelines (NRC, 1983); it was centered within the pool boundaries with the central axis aligned with the long side of the pool.

Each calorimeter was a 6.4-m-long, 1.4-m-o.d., A517 steel pipe with 3.2-cm-thick walls. The calorimeters were fabricated from surplus pipe, which already had 5-cm-thick by 15-cm-wide reinforcing ribs fillet welded to the outside of the pipe on 61-cm centers. At the ends of the pipe, 1.3-cm-thick steel plates, referred to as the end caps, were bolted on to seal the interior of the pipe. Three layers of 2.5-cm-thick Cerablanket insulation were installed against the inner wall of the pipe and against the inside of the end caps.

The east end of the calorimeter was 5.9 m from the east edge of the pool. Instrumentation was located at three axial stations in the calorimeter. Starting from the east end of the calorimeter, Station 1 was 0.46 m away, Station 2 was 2.82 m away, and Station 3 was 5.94 m away. Each station was centered between a pair of exterior ribs. At each axial station, there were four sensor locations on the interior of the pipe. Angular location 000 was on the underside of the calorimeter, then viewing from the east and moving clockwise, angular location 090 faced south, angular location 180 was at the top, and angular location 270 faced north. There was an instrumentation station located at the center of each end cap.

At each location, type K thermocouple wires were spot-welded to the inner surface of the pipe, forming an intrinsic junction. A beaded thermocouple was placed between the first and second layers of insulation. At some stations, multiple thermocouples were used in case of failure. Also, the use of multiple temperature measurements increases the stability and reliability of the estimates of the heat flux from an inverse heat conduction procedure by reducing the effects of random errors from the temperature readings.

To measure flame temperatures, 1.6-mm stainless steel sheathed, ungrounded junction, type K thermocouples were placed at various heights on water-cooled towers arranged about the large calorimeter and 5 cm from the exterior surface at each measurement station on the calorimeter. Three of the towers, named A, B, and C, were 6.1 m high and had thermocouples at 142 cm and 262 cm above the initial fuel level. Five other towers, named *2*, *3*, *4*, *6*, and *7*, were 12.2 m high and had thermocouples at 142 cm, 262 cm, 549 cm, and 1118 cm above the initial fuel surface. Figure 1 shows the placement of the calorimeter and the towers within the pool.

Four small calorimeters, constructed of 1018 mild steel, were installed on tower *3*, which was located to the west of the large calorimeter. Two of these calorimeters were 10.2-cm-dia cylinders and the other two were 20.3-cm-dia cylinders (from this point on referred to as the 10-cm or 20-cm calorimeters). These

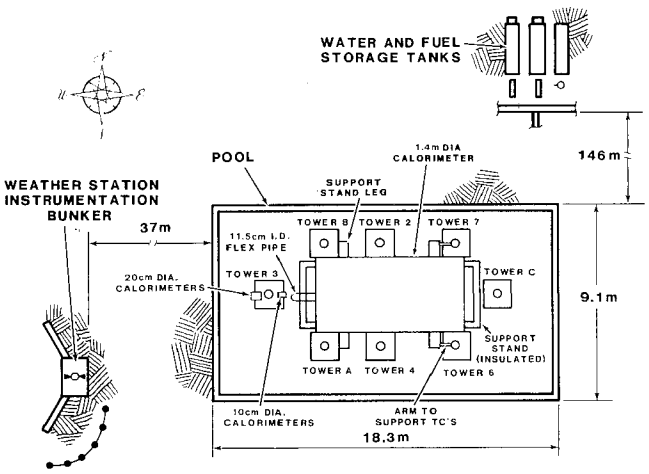

Fig. 1 Plan view of the test facility

Contributed by the Heat Transfer Division and presented at the 24th AIChE/ASME National Heat Transfer Conference, Pittsburgh, Pennsylvania, August 9-12, 1987. Manuscript received by the Heat Transfer Division October 5, 1987. Keywords: Combustion, Fire/Flames.

FSS D00235 R

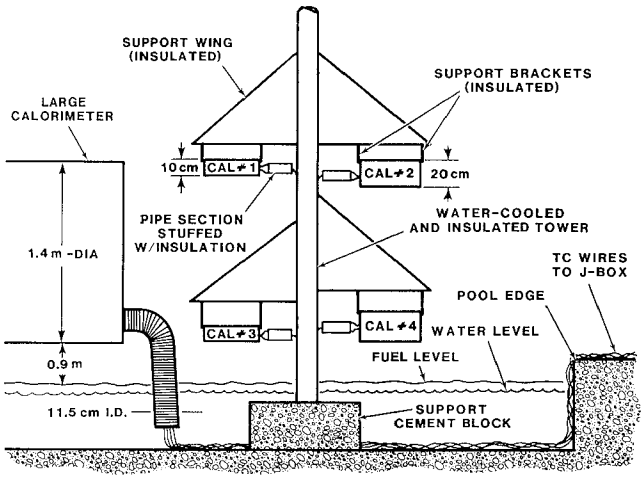

Fig. 2 Placement of small calorimeters in relation to the large calorimeter

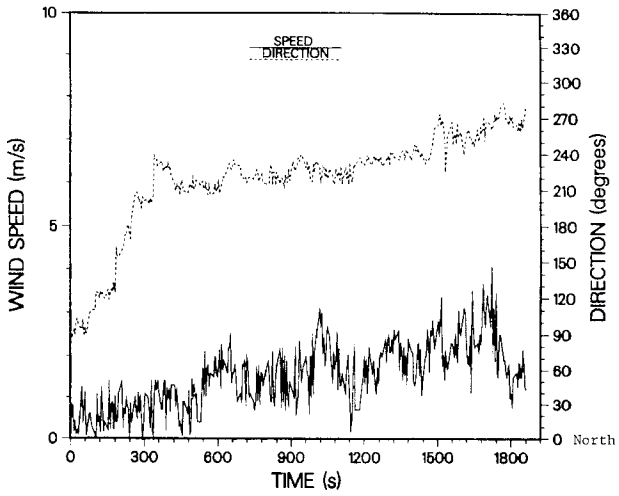

Fig. 3 Wind history for Test C

calorimeters had 3.2-cm-thick walls, were 20.3 cm long, and were cut into four quadrants.

The wall thickness of these calorimeters was the same as that of the large calorimeter. The mild steel was also chosen such that the thermal properties would be similar to those of the larger calorimeter. To reduce circumferential heat conduction between the calorimeter quadrants, a felt insulating strip was placed between them. The interior of each calorimeter was filled with Cerablanket insulation. The whole assembly was held together by 2.5-cm-thick steel caps bolted on both ends of a calorimeter.

Thermocouples were located at the center of each quadrant; these correspond to the angular stations on the large calorimeter. Type K thermocouples were spot-welded (intrinsic junctions) to the inside surface of the cylinder at each station. A beaded thermocouple was placed within the insulating material in the center of the calorimeter, in order to give an internal boundary condition.

The four smaller calorimeters were installed on tower *3* such that their axes were aligned in the same vertical plane as the axis of the large calorimeter. These calorimeters were placed on the tower such that the upper stations of a 10-cm and 20-cm calorimeter lined up with the upper station of the large calorimeter and the lower stations of the other two calorimeters lined up with the lower station of the large calorimeter, as shown in Fig. 2.

Because the wind can drastically change the flow patterns of the fire, an average wind speed of 2 m/s is the upper limit prescribed in the IAEA test specifications. An anemometer, which was located atop the bunker that housed the data logger, served as the instrument for monitoring wind speed and direction.

Test Duration and Fuel Consumption

For the tests, JP-4 aviation fuel was added to 66 cm of water in the pool, where one centimeter depth corresponds to 1670 liters. The depth of fuel added for the first and second tests, tests A and B, was 22 cm, and for the final test, test C, it was 19 cm. Tests A and B were 35 minutes long, while test C was 29 minutes long. The average fuel recession rate for tests A and B was 6.3 mm/min (17.5 liters per second) while that for test C was 6.6 mm/min (18.2 liters per second). These values are in agreement with a nominal fuel recession rate of 6.3 mm/min observed in a number of large pool fires using JP-4 fuel that have been conducted at Sandia.

In comparison, Babrauskas (1983) reports burn rates for gasoline and liquified natural gas pool fires; the values extracted from his plots are 4.3 mm/min for gasoline and 5.8 mm/min for LNG for pools of equivalent diameter, i.e., 14.6 m. Blinov and Khudiakov (1957) give experimental burning rates for gasoline and tractor kerosene; for pool diameters of 9 m and 23 m, the value as reported by Hottel (1959) for both fuels and pool sizes is about 3.8 mm/min.

After the test item and instrumentation were installed and the pool filled, the fuel was ignited by a hand-held torch. The time for the flame front to travel across the surface of the pool along the long axis and fully engulf the large calorimeter was ~ 8 s.

Wind Effects

Large-scale turbulence contributes to the large temporal and spatial fluctuations that characterize the test medium of a large open pool fire. The variable most affecting the conditions in an open pool fire is the ambient wind. The average values and standard deviations of wind speed for each test in this series were 2.0 ± 0.9 m/s, 1.2 ± 0.8 m/s, and 1.5 ± 0.8 m/s for tests A, B, and C, respectively. The prevailing wind direction for test A was from the east by southeast. For test B, the wind prevailed from the southeast, while for test C, the prevailing wind direction was from the southwest. The wind history for Test C is given in Fig. 3.

Wind influences the entrainment patterns in an open pool fire, enhancing air entrainment in some areas. As a result, the temperatures are elevated or depressed depending on local air-to-fuel ratios and efficiency of mixing. Instabilities are enhanced and turbulent flow patterns of the flame are affected. Wake regions are formed downstream of the plume and at times, spiralling vortex flows are seen in the plume at the leeward edges of the pool. Another wind effect is the tilting of the plume such that there were times when the calorimeter, towers and other instrumentation were not fully engulfed by the flames. These wind effects are erratic in nature and contribute to the large spatial and temporal varitaions that were noted within and between tests.

Flame (Gas) Temperature Data

A typical flame temperature history from a tower is shown in Fig. 4 (tower *2*, test C). The data from a single elevation possess large fluctuations, demonstrating the effects of both the characteristic turbulence of a large open pool fire and the wind. The erratic nature of the fire plume is evident from temperature histories. There are variations from tower to tower within a test and variations from test to test.

The mean temperatures were computed for all four measurement locations on each of the five 12.2-m-high towers in

Table 1 Average temperatures from the towers

	Test A				Test B				Test C			
	Test avg, K	Test st dev, K	Low avg, K	High avg, K	Test avg, K	Test st dev, K	Low avg, K	High avg, K	Test avg, K	Test st dev, K	Low avg, K	High avg, K
Twr 2												
e1	1232	107	1212	1254	1264	93	1248	1276	1292	90	1299	1286
e2	1110	121	1061	1163	1089	242	873	1241	1076	213	946	1206
e3	897	215	724	1088	929	265	644	1131	960	265	455	1187
e4	628	232	532	735	811	304	552	995	834	234	694	973
Twr 3												
e1	1065	220	948	1222	****	****	****	****	1204	147	1186	1342
e2	907	353	674	1220	1080	276	909	1391	1020	230	976	1355
e3	856	413	531	1291	812	366	568	1252	611	236	540	1156
e4	904	352	435	1160	693	283	537	974	472	155	426	828
Twr 4												
e1	1189	220	1151	1298	1145	190	1083	1297	1093	168	1078	1159
e2	1084	315	992	1353	997	205	905	1220	****	****	****	****
e3	836	208	731	1147	839	223	713	1147	777	175	704	1094
e4	584	248	470	917	623	244	508	902	569	167	515	804
Twr 6												
e1	1205	167	1194	1257	1102	181	1062	1263	1078	116	1056	1197
e2	1043	196	1002	1250	922	301	832	1288	825	212	758	1193
e3	697	225	606	1162	745	243	641	1165	710	240	620	1210
e4	550	297	439	1120	571	244	473	968	615	235	548	979
Twr 7												
e1	1278	101	1277	1284	1320	106	1317	1323	1252	123	1208	1275
e2	1062	227	1015	1286	1271	193	1160	1443	1269	154	1169	1320
e3	726	248	633	1171	948	268	447	1184	1050	225	794	1181
e4	****	****	****	****	****	****	****	****	****	****	****	****

Notes: **** = no data available; low average = flame "absent"; high average = flame "present"; el = elevation 142 cm; e2 = elevation 262 cm; e3 = elevation 549 cm; e4 = elevation 1118 cm

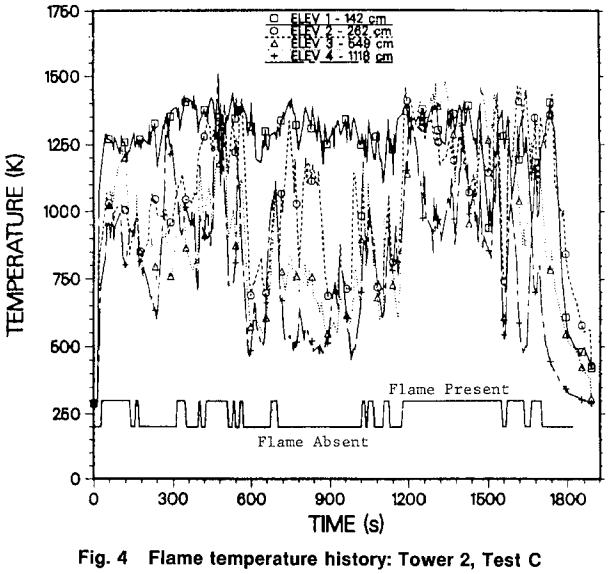

Fig. 4 Flame temperature history: Tower 2, Test C

each test. Table 1 presents these mean temperatures. The average values for elevation 1 range from 1065 to 1320 K, from 810 to 1270 K for elevation 2, from 610 to 1050 K for elevation 3, and from 470 to 905 K at elevation 4. The trend is for the mean temperature to be highest at the lowest elevation and to decrease as the elevation increases. Emphasizing the fact that the dominant wind direction was from the south for all the tests, the towers on the south side of the pool experienced lower mean temperatures. The north towers indicate higher mean values since they may be more centrally located in the plume as a result of the wind-induced tilt.

The standard deviations from the means are also given in Table 1. The trend is for the standard deviations to be smaller at the lowest elevation and to increase as the elevation increases. This is demonstrated by the fact that standard deviations average 12 percent of the mean temperature readings at elevation 1, 23 percent at elevation 2, 31 percent at elevation 3, and 38 percent at elevation 4. The larger spread in temperatures at the upper elevations is expected because at these heights, the wind effects are greater. The average of the mean temperature values obtained at a single elevation from all of the towers in a test agrees with the average values from the other two tests to within 8 percent. This agreement is very good considering the differing ambient wind conditions for each test.

In an attempt to account for wind effects, conditional sampling was used to examine the temperature data. All the data from elevation 4 on the five 12.2-m-high towers for all the tests were gathered. The probability density function of these temperature measurements was found to be bimodal in shape. One mode, at low temperatures, roughly corresponds to data taken when the wind effects were strong. The other mode, at higher temperatures, corresponds to times when the flames engulfed the towers. A setpoint temperature, which corresponded to the local minimum between the peaks of the probability density function, was chosen. This temperature was 935 K. A signal was generated that was high when the temperature was above the setpoint and low when the temperature was below the setpoint. This corresponds to a signal representing the "presence" or "absence" of flames about the towers, as shown in the conditioning signal in Fig. 4. This correspondence is not exact; however, this is a simple starting place to help in examining the fire data.

Statistics were obtained from the conditioned temperature data. The tower temperatures at each elevation were averaged during the flame present and absent periods based on the conditioning signal described above; the results are shown in Table 1. The general trends for these conditional averages are the same as the trends in the total test averages, with the mean temperatures decreasing with elevation. As can be expected, the mean flame present temperature at each elevation is higher than the mean temperature over the entire test at the corresponding elevation. The mean temperatures for the flame present condition are very consistent at the two lower elevations for all of the towers in all of the tests.

The readings obtained for the flame temperature thermocouples are lower than the true flame temperatures. The main

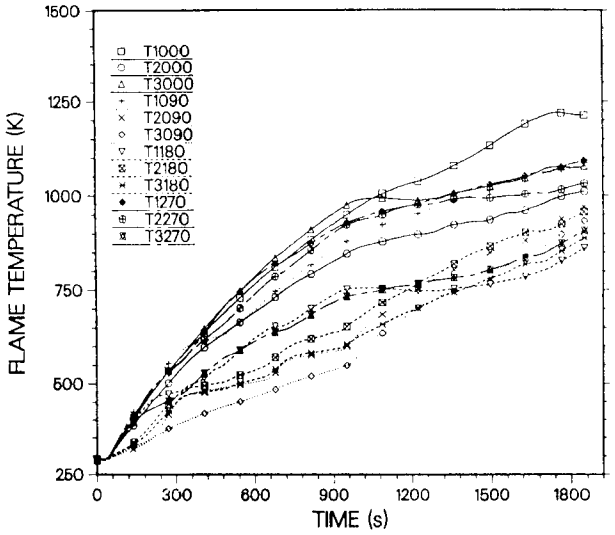

Fig. 5 Steel backface temperature history—Test A

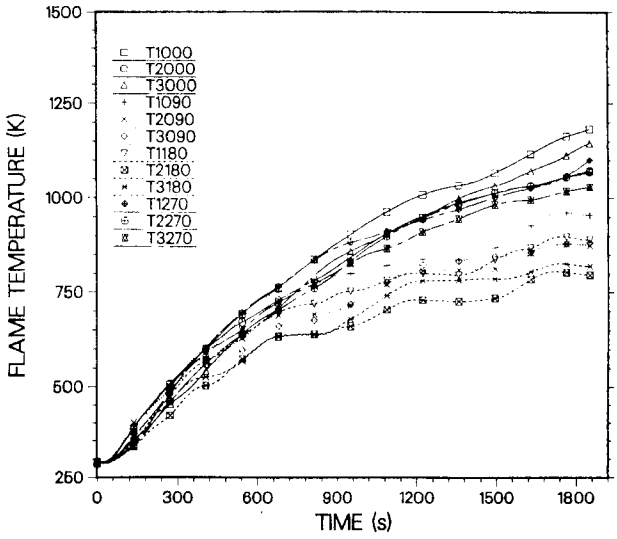

Fig. 6 Steel backface temperature history—Test B

source of error in the readings is believed to be due to radiative heat loss from the thermocopules. The error is probably the greatest for the flame thermocouples that are near the large calorimeter. This occurs because the extinction coefficient in the flames is on the order of 1/m (Longenbaugh, 1988) and these thermocouples are only 5 cm from a large, relatively cool surface. For the thermocouples mounted on the towers, the errors are believed to be small during the flame present condition and will increase during the flame absent condition. Other sources of error include transient effects, soot buildup on the thermocouples, thermocouple calibration, and data system inaccuracies; these errors were not considered in this analysis.

For the thermocouples near the calorimeter, this error is a maximum at the early times in the test and decreases as the calorimeter heats up. The error was estimated from a simplified one-parameter radiative model. The radiative view factors between the thermocouple and both the flames and the large calorimeter were found using the cross-string method with the thermocouple at the cross point. Other assumptions are a nonparticipating gas medium and blackbody radiative exchange between the thermocouple, calorimeter, and fire. Then, by performing a heat balance on a thermocouple assumed to be in radiative equilibrium with the fire at 1255 K and the calorimeter surface, this error is estimated to be approximately 12 percent of the assumed fire temperature when the calorimeter surface is cold (365 K) and 4 percent when the surface is hot (1090 K). This error estimate does not encompass all factors affecting the thermocouple readings.

Method of Obtaining Heat Flux Data

For these tests, the calorimeter backface temperatures were measured; however, the net heat flux at the outer surface is desired. To determine the net heat flux, the temperature data becomes the "boundary condition" in the inverse problem of heat conduction. This problem was solved by a numerical technique presented by Beck et al. (1985). The numerical technique was utilized by Blackwell et al. (1985) to develop a computer code, known as the Sandia One-Dimensional Direct and Inverse Thermal (SODDIT) Code, to generate net heat flux and surface temperature information given interior temperature data.

The calorimeter design was checked in several ways. The use of backface measurements was evaluated in a series of experiments in which a wall section, with multiple frontface and backface thermocouples, was exposed to known radiative heat

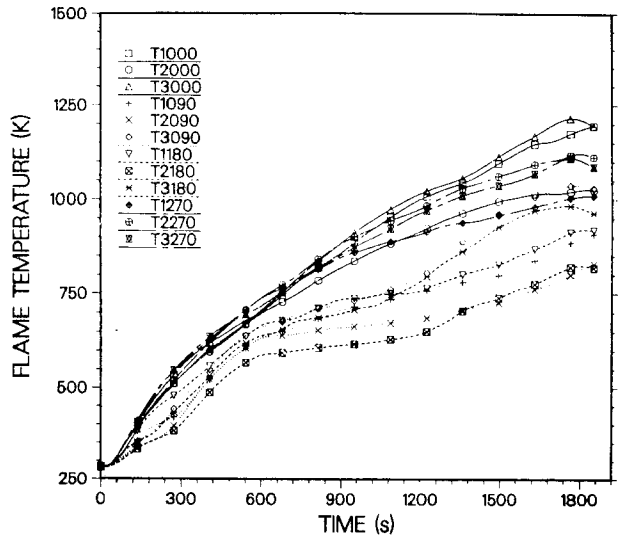

Fig. 7 Steel backface temperature history—Test C

fluxes in Sandia's Radiant Heat Facility. A thermal model was used to show that the local heat conduction was effectively one dimensional.

Because noisy data can promote instabilities in any inverse calculation, a series of simple numerical studies was used to evaluate potential errors. As a result, two approaches were used to reduce the effects of noise in the data analysis procedure. A light smoothing of the actual temperature data was introduced by fitting the data with a smoothing spline with an allowed standard deviation of 0.5 K (a fairly tight fit). An additional smoothing feature in SODDIT is the use of what is termed "future temperature" information, a concept developed by Beck et al. (1985). The future temperature approach allows the use of smaller computational time steps and increases stability. After an extensive review of the data from test A, four future times were chosen to provide calculational stability over the temperature ranges expected in the test series without eliminating the ability to resolve specific thermal events in the tests.

A study of the sensitivity of this inverse procedure to noise in the data was made by analyzing "exact" data to which varying amounts of random noise had been added. The exact temperature data were generated for a triangular heat flux pulse into a planar section of the calorimeter material that had

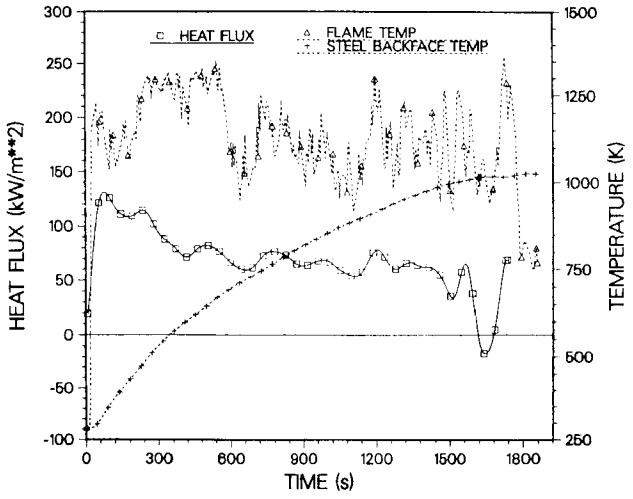

Fig. 8 Net heat flux, steel backface temperature and external flame temperature histories—bottom station

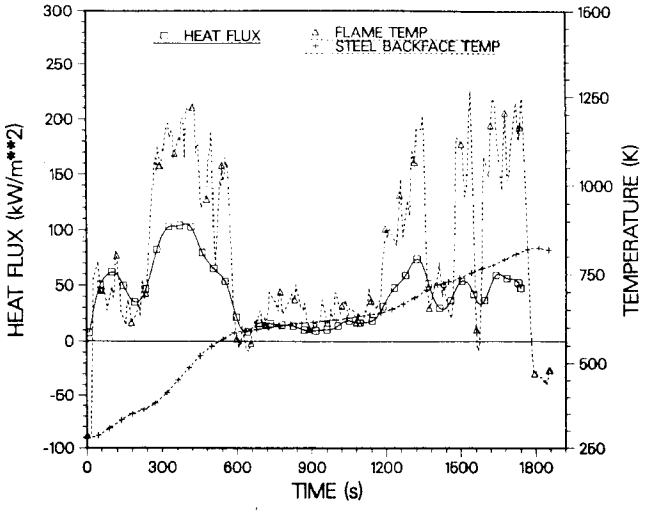

Fig. 10 Net heat flux, steel backface temperature and external flame temperature histories—top station

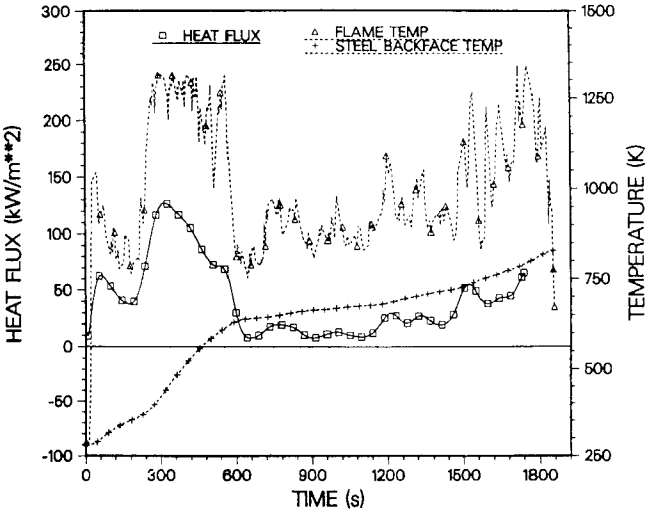

Fig. 9 Net heat flux, steel backface temperature and external flame temperature histories—south station

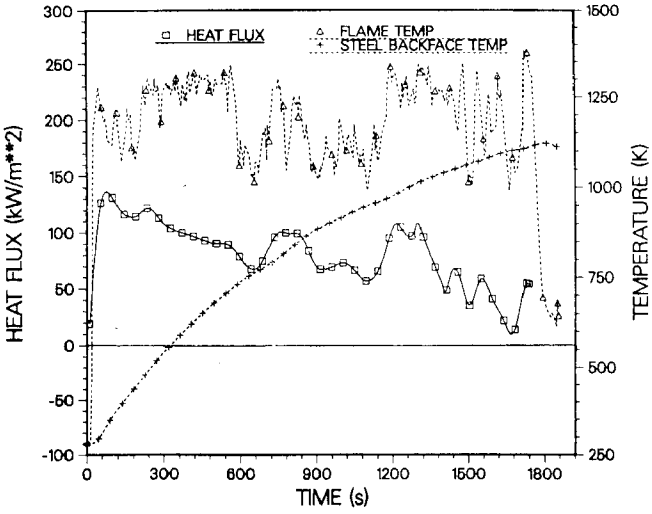

Fig. 11 Net heat flux, steel backface temperature and external flame temperature histories—north station

an insulated backface. Random noise with a standard deviation of 0.05 K to 1.1 K was added to these data. To evaluate any differences in stability as a function of the temperature, the thermophysical properties of the material were evaluated at 530 K or 895 K.

The heat flux profiles calculated from the noisy data sets were compared to the heat flux profile used to generate the exact temperture data. The maximum errors at the lower temperature ranged from 7 percent for the highest noise level to a minimum of 2 percent and then up to 4 percent at the lower noise level. At higher temperature, the values were 17, 4, and 5 percent, respectively. For reference, the random noise in the temperature data taken during the lead-in periods before the tests had a standard deviation of less than 0.03 K.

In spite of the smoothing effects, the heat flux calculations still exhibited oscillations at later times in the tests. This occurs because mild steel experiences a Curie point transition centered at ~ 1035 K. From measurements made on samples taken from the calorimeter wall, this transition is characterized by a sharp spike in specific heat capacity between 975 and 1090 K. Such an abrupt change in thermal properties causes instabilities in the inverse code; the natural fluctuations in the fire temperatures compound the instability problem. As a result, the heat flux calculations at temperatures above the transition temperature are not as reliable. Therefore, when heat flux is presented as a function of surface temperature, data are reported for values less than 1035 K.

Large Calorimeter Heat Flux Data

Temperature histories for all twelve stations are presented in Figs. 5, 6, and 7 for the three tests. These "temperature envelopes" can be used to examine the uniformity in a fire, the integrated heat flux, which is directly related to the total temperature rise, and the repeatability from fire to fire by overlaying the envelopes. A narrower envelope indicates a more uniform thermal exposure over the surface of the calorimeter. This method of comparison is limited to test items with the same thermal properties, wall thickness, and geometry.

For the four stations at the axial center of the large calorimeter, the net heat flux, the steel backface temperature, and the external flame temperature histories from Test C are given in Figs. 8 through 11. Typically, the net heat flux to the calorimeter peaked at test startup, to values between 100 and 160 kW/sq.m, and diminished as the calorimeter surface heated up. The heat flux values naturally tracked the external flame temperature values, but there was a significant amount of filtering. Some of this filtering was due to the natural damping effects of the calorimeter; note the smooth rise of the steel backface temperature curve (thermal response time is on the

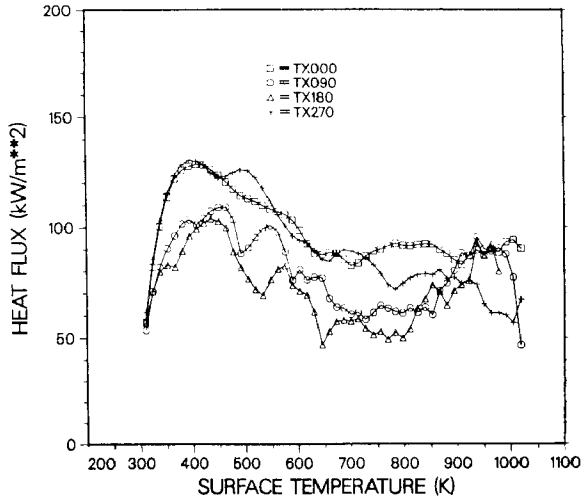

Fig. 12 Average heat fluxes for the test series

order of 9 s). There was additional filtering due to the slight smoothing introduced in preprocessing the data and to the use of future temperature information in the actual data analysis.

The trends in the flame temperatures adjacent to the calorimeter are similar to the trends for the tower flame temperature data. For the southern or 090 station, there were periods of lower values due to wind effects. This also applies to the upper, or 180 station. Videotapes of the test show times when the southern and upper parts of the calorimeter were not fully engulfed in flame; these times correlate with times of low heat flux on the plots. Even though the winds are within the prescribed limits, changes in the winds produce fluctuating, nonuniform temperature fields in the regions around the top and windward side of the large calorimeter.

Temporal data are important in the presentation of the heat flux information, because changes in the heat flux can be correlated with events in the fire, such as fluctuating flame temperatures. From the heat flux histories, total thermal input can be studied and trends within a test defined. Another useful means of data presentation is to plot heat flux as a function of surface temperature. Because the NRC and IAEA test specifications use this format, presentation of the data in this manner facilitates a direct comparison. In this form, thermal transport mechanisms in the fire can also be studied. The SODDIT code provides the estimated surface temperatures for these plots as well as the heat fluxes.

The heat fluxes with respect to angular station, i.e., all the heat flux values from three stations in each of the three tests, were averaged together at specific surface temperature values (note that the time at which a specific temperature is reached is different for each station in a test and from test to test). The mean values are plotted against surface temperature in Fig. 12. The average of the peak fluxes for the lower stations (TX000) and the north stations (TX270) was about 130 kW/sq.m. For the southern stations (TX090), the average of the peak fluxes was 110 kW/sq.m. For the upper stations (TX180), it was 100 kW/sq.m. In general, TX000 exhibited the highest, most uniform peak heat fluxes and TX180, the lowest. Stations TX270, which were on the leeward side of the calorimeter, showed much higher peak heat fluxes than TX090, which were windward during the tests.

Standard deviations from the mean values were computed; they are relatively large for all stations, demonstrating the effects of the wind and the random nature of the fire. Stations TX000 exhibited the smallest values, on the order of 15 percent of the mean. For stations TX270, the standard deviations are on the order of 25 percent, for stations TX090 and TX180, on the order of 35 percent. The stations that had greater exposure to the wind (stations TX090 and TX180) experienced larger fluctuations than the stations that were sheltered from wind effects (stations TX000 and TX270). From the visual data, the south side of the calorimeter could actually be seen at times during all three tests. Even when the plume engulfed the test item, the flame thickness was not as great on the windward and upper stations of the calorimeter; this lowers the radiative transport to these portions of the calorimeter.

Table 2 Integrated heat flux at 30 min* (kw-hr/sq. m)

Test	Angle, deg	Station 1 (East)	Station 2 (Middle)	Station 3 (West)
A	0	43.8	32.0	37.5
	90	38.2	28.8	26.4
	180	22.5	28.1	24.0
	270	38.5	34.5	25.0
	End Cap	18.3	*****	19.6
B	0	42.3	37.3	41.0
	90	28.2	23.6	23.6
	180	24.3	19.8	20.7
	270	38.5	37.3	33.9
	End Cap	19.6	*****	20.6
C	0	42.8	33.3	43.4
	90	25.7	21.4	33.5
	180	26.1	20.8	29.6
	270	33.7	39.1	38.3
	End Cap	21.6	*****	18.8

*Test C was only 29 min, so values were extrapolated to 30 min.

Table 3 Statistics for the integrated heat flux at 30 min* (kw-hr/sq. m)

Cylindrical surface	Low	Mean	High	Standard deviation, percent
Test A—All	22.5	31.6	43.8	6.8 (21.5)
Test B—All	19.8	30.9	42.3	8.3 (26.9)
Test C—All	20.8	32.3	43.4	7.7 (23.8)
Station 1—All	22.5	33.7	43.8	7.9 (23.4)
Station 2—All	19.8	30.0	39.1	6.9 (23.0)
Station 3—All	20.7	31.4	43.4	7.6 (24.2)
0 deg—All	32.0	39.3	43.8	4.4 (11.2)
90 deg—All	21.4	27.7	38.2	5.3 (19.1)
180 deg—All	19.8	24.0	29.6	3.4 (14.2)
270 deg—All	25.0	35.4	39.1	4.5 (12.7)
End Caps—All	18.3	19.8	21.6	1.2 (6.1)

*Test C was only 29 min, so values were extrapolated to 30 min.

Integrated heat flux values at 30 min are presented for the test series in Table 2. Statistics for these values are presented in Table 3. High, low, and mean values, as well as standard deviations from the mean, are provided for various groups of data. The data are grouped as follows: all cylindrical surface data with respect to test, all data for the series with respect to axial station, all data for the series with respect to angular station, and all end cap data for the test series. Note that there is approximately a two-to-one ratio between the high and low values for the first and second groupings and the standard deviations are about 25 percent. When grouped with respect to angular station, however, the spread and the standard deviations are smaller.

Small Calorimeter Heat Flux Data

Heat flux histories for the 10-cm and 20-cm calorimeters from Test C are presented in Figs. 13 through 16 along with the closest flame temperatures located above each calorimeter. For the lower calorimeters, these flame temperatures were measured ~50 cm above the upper stations and for the upper calorimeters, ~25 cm above the upper stations. The fluctuations in heat flux for the smaller calorimeters were generally greater than for the large calorimeter. This phenomenon is believed to be due to the fact that the large calorimeter damps

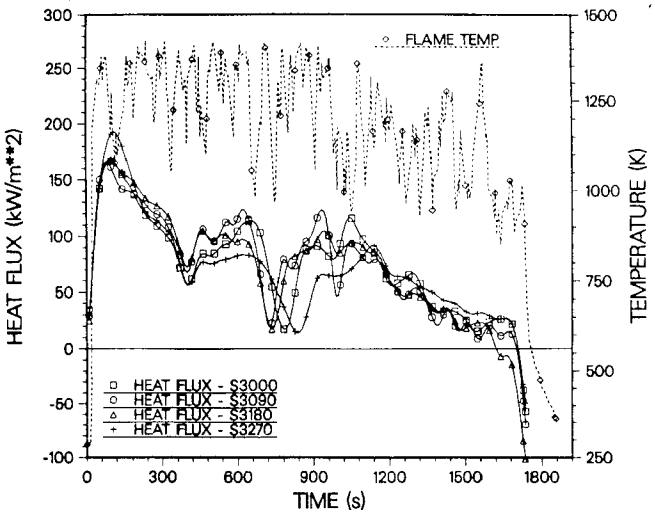

Fig. 13 Heat flux and flame temperature histories: lower 10-cm calorimeter

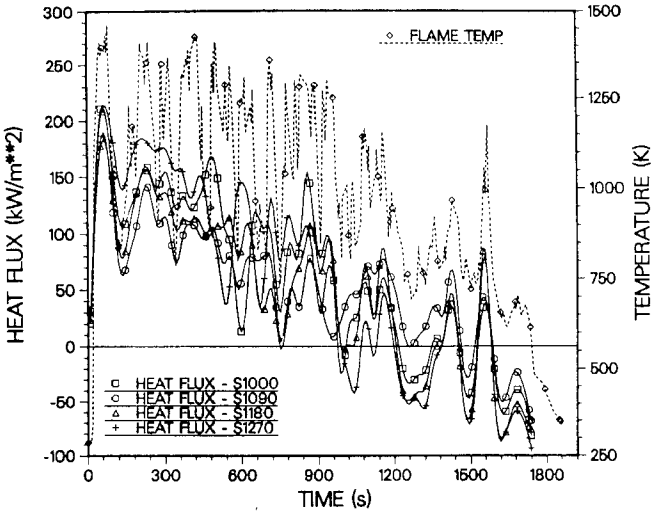

Fig. 15 Heat flux and flame temperature histories: upper 10-cm calorimeter

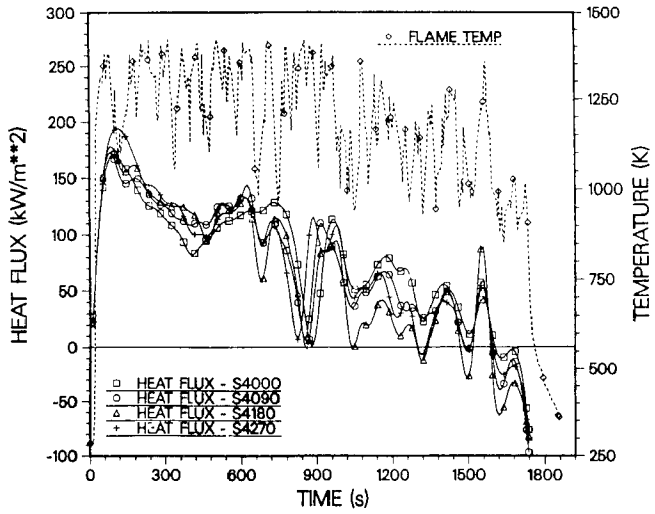

Fig. 14 Heat flux and flame temperature histories: lower 20-cm calorimeter

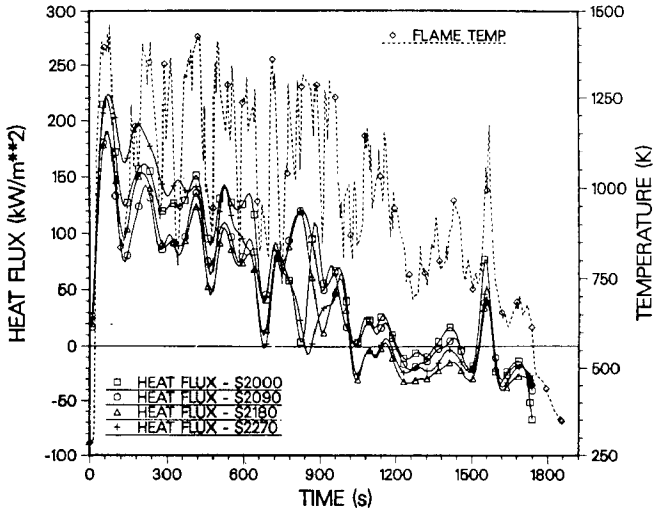

Fig. 16 Heat flux and flame temperature histories: upper 20-cm calorimeter

out the local temperature variations in the flame to a greater degree. Peak fluxes for the smaller calorimeters were generally between 160 and 200 kW/sq.m, with the exception of the upper calorimeters in test A. These calorimeters experienced relatively low fluxes for the first half of the test.

Typically, the trends in the heat flux histories from all angular stations for a single calorimeter track each other. For the upper calorimeters, however, the heat flux values differ by as much as a factor of two from one station to the next on a single calorimeter.

There are general trends for the angular variation in heat fluxes; station 270, on the leeward side, demonstrates the highest heat fluxes. The bottom station 000 follows closely, and as on the larger calorimeter, the upper and windward stations (180 and 090) demonstrate lower fluxes. The heat flux values for the small calorimeters in test A are in general lower than those in the other tests, a result of the generally lower local flame temperatures at the west end of the pool.

Discussion of Results

Heat Flux Data. On the large calorimeter, the circumferential variations in the heat flux and the integrated heat flux are probably the result of several phenomena. Fluctuating, nonuniform temperature fields due to the wind effects have been previously noted; there is a steady decrease in the average temperature with increasing elevation. Wind effects on the heat fluxes at the top and windward stations are readily apparent. Even with no wind, the variations in the convective heat transfer are significant; for a cylinder in crossflow, the local heat transfer coefficients are highest at the lower stagnation point, decrease appreciably at the sides, and then increase up to the top of the cylinder. Because the calorimeter is a massive heat sink (the maximum absorption rate was approximately 5 MW), a cooler, soot-laden boundary layer probably exists around the calorimeter; this boundary layer is believed to act as a radiation shield.

There is evidence of domelike fuel-rich vapor regions above the fuel surface in small pool fires. Corlett (1974) described pool fires of more than 1 m diameter as being "unstructured" flames with no large, cold, fuel-rich vapor dome. If the vapor dome was present in the fires in this test series, then the lowest heat flux levels would be at the 000 stations on the underside of the large calorimeters, due to a decrease in the radiant field intensity. The fact that the heat flux values are highest at the 000 stations indicates that no large vapor dome is present.

There have been studies that predict the radiant heat transfer to a horizontal cylinder engulfed in luminous flames (Birk and

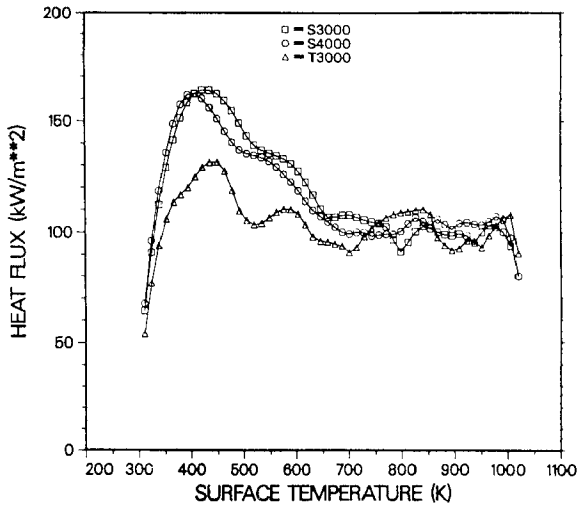

Fig. 17 Average heat flux versus surface temperature: lower stations, large and small calorimeters

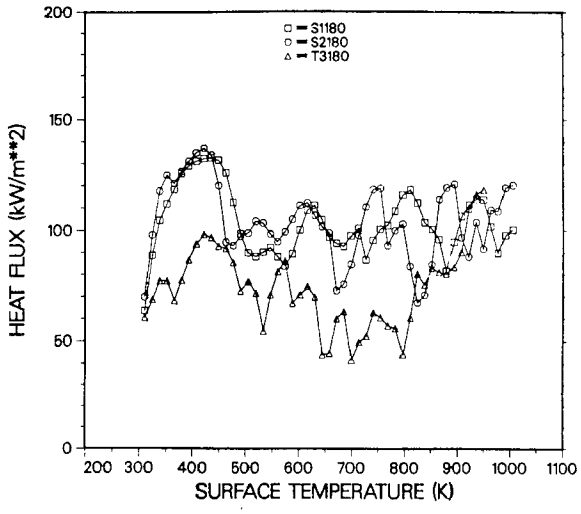

Fig. 18 Average heat flux versus surface temperature: upper stations, large and small calorimeters

Oosthuizen, 1982; Tunc and Karakas, 1985). Because there are insufficient data to define the temperature field in the flame volume, the flame is considered as a participating medium with a uniform temperature and extinction coefficient. The size of the fire and the positioning of the cylinder in the fire will strongly affect the predicted heat flux distribution. Formulations were done for cases in which the bottom of the cylinder was 0.3 m and 1 m above the pool and the width of the pool perpendicular to the cylinder axis was between 2.4 m and 7.6 m. Probably as a result of the assumption of a uniform flame temperature, these analyses predict that the highest heat fluxes will be at the top and the values will decrease along the periphery to the underside of the cylinder. The data in Table 1 show that the average temperature decreases with increasing elevation. The lowest net fluxes are measured at the top of the calorimeter (stations 180) and the highest fluxes are measured on the underside of the calorimeter (stations 000).

Because only total heat flux measurements were made in these tests, an attempt was made to estimate the radiative/convective partitioning of heat transfer to the calorimeters during the periods of low winds. Using data from Schneider and Kent (1987) for measurements made in the same pool but in a different test, the average velocity was 4.8 m/s at an elevation of 1.4 m above the initial fuel surface. This was slightly above the location of the bottom stations on the large calorimeter and the lower 10-cm and 20-cm calorimeters. Using this velocity, the convective heat transfer coefficients at the stagnation point were calculated for the three cylinders in cross-flow. The coefficients were computed for surface temperatures of 420 K, the temperature at which the peak flux occurs in Fig. 17, and a flame temperature of 1200 K, which is approximately the average temperature from Table 1 at this elevation. For these conditions, the Grashof number for the large calorimeter is 3.8×10^9 and the Reynolds number is 80,500. Assuming that the gas is air, the average Nusselt number is 120 for natural convection and 213 for forced convection. Kreith (1963) indicates that turbulent, forced convection should be assumed for these conditions.

Using correlations for forced convection from Kreith (1963), the stagnation point convective fluxes were 8.5, 22, and 32 kW/sq.m. for the 1.4-m, 20-cm, and 10-cm calorimeters, respectively. For the test series, the average total heat fluxes estimated by SODDIT at these stations, for surface temperatures of 420 K, were 130, 170, and 170 kW/sq.m. Thus, the convective flux was estimated to be 6.5, 13, and 19 percent of the total cold wall flux for the calorimeters.

The variation in the forced convection heat transfer coefficient around the large calorimeter was calculated for the conditions listed above. The approximate values of the local Nusselt number are 280 at station 000, 130 at stations 090 and 270, and 210 at station 180.

The velocity field is strongly correlated with the temperature field (McCaffrey, 1979; Schneider and Kent, 1987; Weckman, 1987). Because the flow is buoyancy dominated, the velocity will drop when the temperature drops. However, the heat transfer coefficient remains approximately constant because temperature-dependent changes in the gas properties roughly offset the effects of the changes in the gas velocity. Using the temperature and velocity measurements in Schneider and Kent (1987), the calculated heat transfer coefficient varied by less than 15 percent over a temperature range of 775 to 1275 K using the assumption of turbulent flow over a cylindrical body.

The convective heat transfer to a flat plate in parallel flow was also calculated. The analysis used the same conditions as above. The elevation of 1.4 m is slightly below the instrumentation stations on the end plates of the large calorimeter. For these conditions, the local Reynolds number is 39,300. Although the Reynolds number is below the level where the flow over a flat plate is normally considered to be turbulent, a turbulent flow correlation was used to estimate the heat transfer coefficient because the incoming or free-stream flow is believed to be turbulent.The convective flux estimate was 7 kW/sq.m. The average total heat flux estimated by SODDIT on the end plates for a surface temperature of 420 K was 108 kW/sq.m; thus, of the total cold wall heat flux to the end plates, ~7 percent is convective, and the balance radiative.

Large Versus Small Calorimeters. As shown in Fig. 2, the small calorimeters were placed with either top or bottom stations at the same elevation as the corresponding stations on the large calorimeter. Three sizes were used in an attempt to compare the heat transfer to objects of different size and total thermal capacity. The stations of interest on the large calorimeter are the bottom west station, T3000, and also the top west station, T3180. The stations from the 10-cm and 20-cm calorimeters are the bottom stations of the lower calorimeters, stations S3000 and S4000, and the top stations of the upper calorimeters, S1180 and S2180. The heat flux was averaged for each station for all three tests with the results plotted for the lower stations in Fig. 17 and for the upper stations in Fig. 18.

The average heat flux curves for the lower stations in Fig. 17 are relatively smooth. The peak flux of 130 kW/sq.m to the 1.4-m calorimeter is about 80 percent that of the peak

fluxes of 164 kW/sq.m to the 10-cm and 20-cm calorimeters. The magnitudes of the fluxes to the 10-cm and 20-cm calorimeters are roughly equivalent throughout the temperature range, and above approximately 700 K, all three curves converge to the same values.

The average heat flux curves for the upper stations in Fig. 18 fluctuate a great deal more than for the lower stations, and the magnitudes of the fluxes are noticeably smaller. The lower heat fluxes and large fluctuations probably result from wind effects. The peak flux of 90 kW/sq.m to the large calorimeter is two thirds that of the peak fluxes of 135 kW/sq.m to the smaller calorimeters. The peak fluxes to the 10 cm and 20 cm calorimeters are almost equal in magnitude but 18 percent below the fluxes to the lower calorimeters reported above.

A conditional analysis of the heat flux data from the large calorimeter was reported by Bainbridge and Keltner (1987). In this type of analysis, a subset of the data is obtained in which the wind effects are minimal; this allows estimates of the heat transfer when the calorimeter is fully engulfed by the flames. The analysis shows the same type of heat flux distribution: maximum on the bottom and minimum on the top.

The phenomena noted here support the postulation of an interaction between an object and the fire that surrounds it. The large calorimeter appears to alter this interaction because it is physically large and thermally massive. This indicates that the heat transfer to an object engulfed in a fire can be highly dependent on the properties of the item.

Summary

A series of large fire tests was conducted to supply information about the thermal exposure of a large object immersed in a fire and the repeatability of the thermal environment. Thermal measurements have been presented from three large open pool fire tests run with duplicate instrumentation. Heat flux and temperature data within the lower part of the fire have been studied in a variety of ways and the strong influence of the wind has been noted. Statistics have been developed to evaluate the test-to-test repeatability of the fire environment.The largest factor affecting the reproducibility of the environment in a large open pool fire is the wind.

Average flame temperatures at eight locations around the test item ranged from 1065–1320 K at a height of 142 cm and from 810–1270 K at a height of 262 cm above the initial pool surface. The spread in these values is quite large. When the temperatures are averaged for all eight locations in each test (a larger sample size), however, the spread in values decreases. For elevation 142 cm, averages for tests A, B, and C, respectively, were 1195, 1210, and 1185 K; these values are within 2 percent of each other. For elevation 262 cm, the average values were 1040, 1070, and 1050 K; these values are within 3 percent of each other.

The peak heat fluxes to the large test item for various locations on the item ranged from 100–160 kW/sq.m. The fluxes to the underside of the calorimeter were highest and those at the top were the lowest; this distribution is counter to the heat flux distributions predicted with simplified radiation modeling that assumes uniform flame temperatures. When averaged for all locations, the peak flux for each test was between 115 and 120 kW/sq.m.

The partitioning of the peak heat flux to the bottom location of the cylinders in crossflow was estimated to range from 6.5 to 19 percent convective with the balance radiative. The magnitude of the convective contribution is size dependent; the larger the radius of the cylinder, the lower the convective contribution to the total flux. For flat plates in parallel flow, the partitioning of the heat transport was estimated to be 6 percent convective with the balance radiative.

The total heat input or the time-integrated heat flux values for the test item were determined. The values for a single test varied with respect to location by as much as a factor of two; again, the highest values were on the bottom and lowest on the top. When all stations were averaged for a single test, the values of 31.6, 30.9, and 32.3 kW-hr/sq.m for tests A, B, and C, respectively, were within 5 percent of each other.

The physical size and thermal capacitance of a test item affect the level of thermal exposure in a fire. The effects are demonstrated when heat fluxes to the large test item are compared with the heat fluxes to smaller items in the fire. The average peak fluxes to a large calorimeter are about 75 percent of those to much smaller calorimeters.

Acknowledgments

The test program was funded by the Federal Rail Administration of the U.S. Department of Transportation (DOT). Sandia National Laboratories is operated by AT&T Technologies for the U.S. Department of Energy (DOE) under Contract No. DE-AC04-76DP00789.

References

Babrauskas, V., 1983, "Estimating Large Pool Fire Burning Rates," *Fire Technology*, Vol. 19, No. 4, pp. 251–261.

Bainbridge, B. L., and Keltner, N. R., 1987, "Heat Transfer to Large Objects in Large Pool Fires," International Conference on Major Hazards in the Transport and Storage of Pressure Liquified Gases, University of New Brunswick, Aug.; proceedings to be published in the *Journal of Hazardous Materials*.

Beck, J. V., Blackwell, B. F., and St. Clair, C. R., Jr., 1985, *Inverse Heat Conduction, Ill-Posed Problems*, Wiley, New York.

Birk, A. M., and Oosthuizen, P. H., 1982, "Model for the Prediction of Radiant Heat Transfer to a Horizontal Cylinder Engulfed in Flames," ASME Paper No. 82-WA/HT-52.

Blackwell, B. F., Douglass, R. W., and Wolf, H., 1985, "A User's Manual for the Sandia One-Dimensional Direct and Inverse Thermal (SODDIT) Code," SAND 85-2478, Sandia National Laboratories, Albuquerque, NM.

Blinov, V. I., and Khudiakov, G. N., 1957, "Certain Laws Governing Diffusion Burning of Liquids," *Doklady Akademii Nauk SSSR*, Vol. 113, pp. 1094–1098.

Corlett, R. C., 1974, "Velocity Distributions in Fires," *Heat Transfer in Fires*, Wiley, New York, pp. 239–255.

Gregory, J. J., Mata, R., Jr., and Keltner, N. R., 1987, "Thermal Measurements in a Series of Large Pool Fires," SAND 85-0196, Sandia National Laboratories, Albuquerque, NM.

Hottel, H. C., 1959, "Review: Certain Laws Governing the Diffusive Burning of Liquids," *Fire Research Abstracts and Reviews*, Vol. 1, pp. 41–43 (translated from Blinor, X. X., and Khudiakor, Y. Y., 1957, *Dokl. Akad. Nauk SSR*, Vol. 113, p. 1096).

IAEA, 1985, "Regulations for the Safe Transport of Radioactive Materials," Safety Series No. 6 of the International Atomic Energy Agency Safety Standards, Paragraph A628.11 "Fire Conditions," Advisory Material on Paragraph 628—"The Thermal Test," rev. ed., Vienna, STI/PUB/323.

Kreith, F., 1963, *Principles of Heat Transfer*, International Textbook Co., Scranton, PA.

Logenbaugh, R. S., 1985, "Experimental and Theoretical Analysis of the Radiative Transfer Inside of a Sooty Pool Fire," Master's Thesis, New Mexico State University; SAND 86-0083, Sandia National Laboratories, Albuquerque, NM, 1988.

McCaffrey, B. J., 1979, "Purely Buoyant Diffusion Flames: Some Experimental Results," NBSIR 79-1910, National Bureau of Standards, Washington, DC.

NRC, 1983, "Packaging of Radioactive Material for Transport and Transportation of Radioactive Material Under Certain Conditions," U.S. Nuclear Regulatory Commission, Title 10, Code of Federal Regulations, Part 71.

Schneider, M. E., and Kent, L. A., 1987, "Measurements of Gas Velocities and Temperatures in a Large Open Pool Fire," *Heat and Mass Transfer in Fires*, ASME-HTD-Vol. 73; to be published in *Fire Technology*.

Tunc, M. M., and Karakas, A., 1985, "Three-Dimensional Formulation of the Radiant Heat Flux Variation on a Cylinder Engulfed in Flames," ASME JOURNAL OF HEAT TRANSFER, Vol. 107, pp. 949–952.

Weckman, E. J., 1987, "The Structure of the Flowfield Near the Base of a Medium-Scale Pool Fire," Ph.D. Dissertation, University of Waterloo, Waterloo, Ontario, Canada.